Article

Statistical Modeling of the Machinability of an In-Situ Synthesized RZ5/TiB$_2$ Magnesium Matrix Composite in Dry Turning Condition

Arabinda Meher [1,*], Manas Mohan Mahapatra [2], Priyaranjan Samal [3], Pandu Ranga Vundavilli [2] and Karthik Venkitraman Shankar [4]

1 Department of Mechanical Engineering and University Centre for Research & Development, Chandigarh University, Mohali 140413, Punjab, India
2 School of Mechanical Sciences, Indian Institute of Technology Bhubaneswar, Kansapada 752050, Odisha, India
3 Department of Mechanical Engineering, Koneru Lakshmaiah Education Foundation, Vaddeswaram 522302, Andhra Pradesh, India
4 Department of Mechanical Engineering, Amrita Vishwa Vidyapeetham, Amritapuri 690525, Kerala, India
* Correspondence: am39@iitbbs.ac.in; Tel.: +91-87-6339-6357

Abstract: Machinability analyses of metal matrix composites are essential for manufacturing industries. The current study is focused on the mathematical modeling of the machinability of an in-situ synthesized RZ5-8 wt.% TiB$_2$ composite using the Taguchi design statistical tools and analysis of variance (ANOVA). Taguchi's method indicates that the feed rate is the most influential parameter, followed by the depth of cut and cutting speed in determining the cutting force and surface roughness during the machining of the RZ5/8 wt.% TiB$_2$ composite. A regression analysis of the experimental data was carried out using ANOVA, and regression equations were established to estimate cutting force and surface roughness under different parametric conditions. The regression model was validated for other test conditions and the maximum deviation observed was ±10%. Main effects plots and response surface plots were developed to analyze the machining parameters' individual and combined effects on the RZ5/8 wt.% TiB$_2$ composite's machinability. The chip morphology and tool wear of the RZ5/8 wt.% TiB$_2$ composite were analyzed using FESEM under different machining conditions.

Keywords: machinability; Taguchi design; regression model; cutting force; surface roughness

1. Introduction

Magnesium is the lightest material for high-volume structural applications in the automotive and aviation industries. The lower density of magnesium helps to enhance energy efficiency and reduce flue emissions compared to steel and aluminum [1]. Commercially available magnesium and its alloys have relatively lower strengths. The strengths of the materials can be improved by incorporating ceramic reinforcements, such as Al$_2$O$_3$, B$_4$C, SiC, TiB$_2$, WC, etc. [2,3]. The reinforcement particles can be added to the matrix using different processing routes, such as liquid metallurgy, infiltration, powder metallurgy (P/M), friction stir processing (FSP), and the cold spray technique [4–6]. Composite synthesis using the stir casting process is the most economical for high-volume structural applications. The reinforcement can be embedded into the magnesium matrix by an ex-situ process (pre-synthesized reinforcement introduced into the matrix phase) or an in-situ process (reinforcement synthesized during the synthesis of the composite) [7,8]. In-situ synthesized composites have improved mechanical and tribological properties due to their better wettability, thermally stable reinforcement, and strong reinforcement-matrix interfacial bonding [9]. Adding reinforcement to the metallic matrix augments the properties of the materials, improving hardness, tensile strength, impact strength, and wear resistance [10,11].

The metal matrix composites synthesized by different processing routes are of near-net shape. The machining of composites is necessary for various industrial applications. However, the presence of reinforcement affects the machinability of the materials due to the existence of two or more distinct phases having significantly different properties [12,13]. During the machining of materials, cutting tools encounter two different phases (one has high ductility and toughness, while the other has very high strength and brittleness). Turning is the most common machining process to achieve a net-shaped product with the dimensional accuracy of the developed material. The machinability of the materials by turning is controlled by machining parameters (cutting speed, feed rate, and depth of cut), cutting tool geometry, and machining environment (with/without cutting fluid) [14–17].

The selection of machining parameters plays a significant role in achieving improved machinability properties. Pramanik et al. investigated the effect of machining parameters on the machinability of metal matrix composites. During the turning of the materials, it was observed that the cutting force of the materials significantly increased with an increase in feed rate. However, it was minimally affected by the cutting speed and reinforcement content. The surface roughness of the materials was controlled by fracture and pull-out of reinforcement at a lower feed rate. The presence of ceramic reinforcements also increased the chips' breakability [18]. Anandakrishnan and Mahamani investigated cutting force, surface roughness, and tool wear in the machining of Al6061-TiB_2 metal matrix composites. It was observed that higher TiB_2 reinforcement minimized the cutting force and increased the surface roughness and tool wear. The cutting force, surface roughness, and tool wear of the materials increased with an increase in feed rate and depth of cut due to the generation of high frictional heating [19].

The machining parameters and environment must be optimized to meet industrial requirements [20]. The cutting force during machining and the surface roughness of the machined surface can be minimized by optimizing multiple performance characteristics of the different response parameters. The optimization can be achieved using lower-the-better quality characteristics to improve the machinability of materials [21]. Kumar et al. optimized the machining parameters for dry turning of Ti4Al6V using the Gray–Taguchi approach. It was observed that the feed rate and cutting speed significantly affected the material's overall machining performance. ANOVA analysis of the machining parameters indicated that cutting speed, feed rate, and depth of cut affected the performance characteristics by 37.42, 46.84, and 14.94%, respectively. The tool wear indicated both abrasive and adhesive wear during the turning of the Ti4Al6V. Abrasive wear occurred on the flank face due to the friction between the face of the cutting tool and the machined part, whereas adhesive wear occurred due to the thermal softening of the tooltip at a higher cutting speed [22].

Karloopia et al. analyzed the machinability of in-situ synthesized Al-Si-TiB_2 composites. It was observed that at a constant cutting speed, feed force and cutting force increased with an increase in feed rate at each depth of cut. Machining the Al-Si-TiB_2 composites at a lower feed rate and cutting speed generated discontinuous chips of shorter lengths. In contrast, helical chips were produced at a higher feed rate and cutting speed. The two-degree model accurately predicted feed force, cutting force, and surface roughness with a lower error range (3−9%) [23]. Khanna et al. machined an AZ91/SiC particulate magnesium matrix composite and analyzed the surface roughness and chip breakability index through a full factorial experimental design. The ultrasonic-assisted turning of the AZ91/SiC composite was better than the conventional process in terms of surface roughness. The machining parameters were optimized through regression analysis and the Jaya algorithm to achieve a better surface finish in the different cutting environments [24]. Kök et al. analyzed the (R_a) surface roughness characteristic during the machining of 2024Al/Al_2O_3 composites and mathematically modeled the behavior using ANOVA and the Taguchi method. Machining of the materials was performed using K10 and TP30 carbide-tip tools. The surface roughness value was higher for the surface machined using the K10 tool than the surface machined using the TP30 tool. An ANOVA model was established for surface roughness,

and it was observed that the errors associated with the K10 and TP30 tools were 1.67% and 4.94%, respectively, with good agreement between the predicted and the experimental results [25].

Ghandehariun et al. established a constitutive model to understand the behavior of metal matrix composites during machining. The constitutive model was established by varying its main features, such as reinforcement size and volume fraction. The energy-based force model was validated through different machining experiments with variations of cutting speed and feed rate, with near-accurate prediction [26]. Wang et al. developed a mathematical model for predicting the cutting force during SiC/Al composite machining based on both the geometrical and mechanical properties of cutting tools and workpiece materials. The value of the expected cutting force component closely agreed with the experimental results in most machining conditions [27]. Gürbüz et al. investigated the machining properties of AISI 4140 steel both experimentally and statistically with the variation of cutting parameters and environments. It was observed that tool wear was minimal when machining the materials using minimum quantity lubrication (MQL). The machining force increased with an increase in feed rate and decreased with an increase in cutting speed. However, the surface roughness increased with an increase in feed rate and decreased with an increase in cutting speed. The statistically predicted machinability behavior was observed to show good coherence with the experimental outcome. Optimizing the cutting and vibration parameters through the statistical model generated a surface finish of 0.413 µm [28].

The literature shows that metal matrix composites possess improved mechanical and tribological properties compared to conventional alloys. However, the machinability of materials is significantly affected by the presence of two different phases. Better machinability of materials can be obtained by selecting the proper machining parameters. Optimizing machining characteristics is necessary, and very few studies have optimized the machinability of materials. In the present study, experimental data for cutting force and surface roughness obtained during the machining of an RZ5/8 wt.% TiB_2 composite were statistically analyzed using a full factorial experimental design. Main effects plots and response surface plots were used to investigate the individual and combined effects of the machining parameters. The established regression model was validated through a series of test cases. The chip morphology and tool wear of the composite were analyzed using a field emission scanning electron microscope (FESEM).

2. Materials and Methods

2.1. Materials Synthesis

Magnesium RZ5/TiB_2 in-situ metal matrix composites were synthesized using the self-propagating high-temperature synthesis (SHS) route. Ti mesh and boron powder were used to synthesize the TiB_2 reinforcement in the molten RZ5 alloy matrix while synthesizing RZ5/TiB_2 composites. The detailed synthesis process for the RZ5/TiB_2 composites is explained in our earlier study [29]. Among the synthesized composites, the RZ5/8 wt.% TiB_2 composite showed improved mechanical properties compared to RZ5/(4 and 6) wt.% TiB_2 reinforced composites. The RZ5/8 wt.% TiB_2 composite samples were prepared with lengths of 250 mm and diameters of 50 mm to study the machinability behavior.

2.2. Machinability Analysis of the Material

The RZ5/8 wt.% TiB_2 composite was machined using an NH 22 lathe (Hindustan Machine Tools manufacturer, Bengaluru, India). The cutting force during machining was measured using a Kistler piezoelectric dynamometer (Type – 9157B). The cutting force data were recorded through a data acquisition system connected to a charge amplifier using DynoWare software. Figure 1 shows a photograph of the experimental setup. The cutting force was measured with variations in cutting speed, feed rate, and depth of cut. The cutting force of the materials was measured twice for each parametric condition, and average surface roughness is reported. Each measurement was performed using a new

cutting edge of a carbide-tip cutting tool manufactured by Sandvik Coromant (CNMG 12 04 08-SM, H13A). The machinability of the materials was also measured in terms of surface roughness. The surface roughness was measured using the surface roughness tester manufactured by Mitutoyo (Surftest SJ-210). Surface roughness was measured twice, and the average surface roughness is reported.
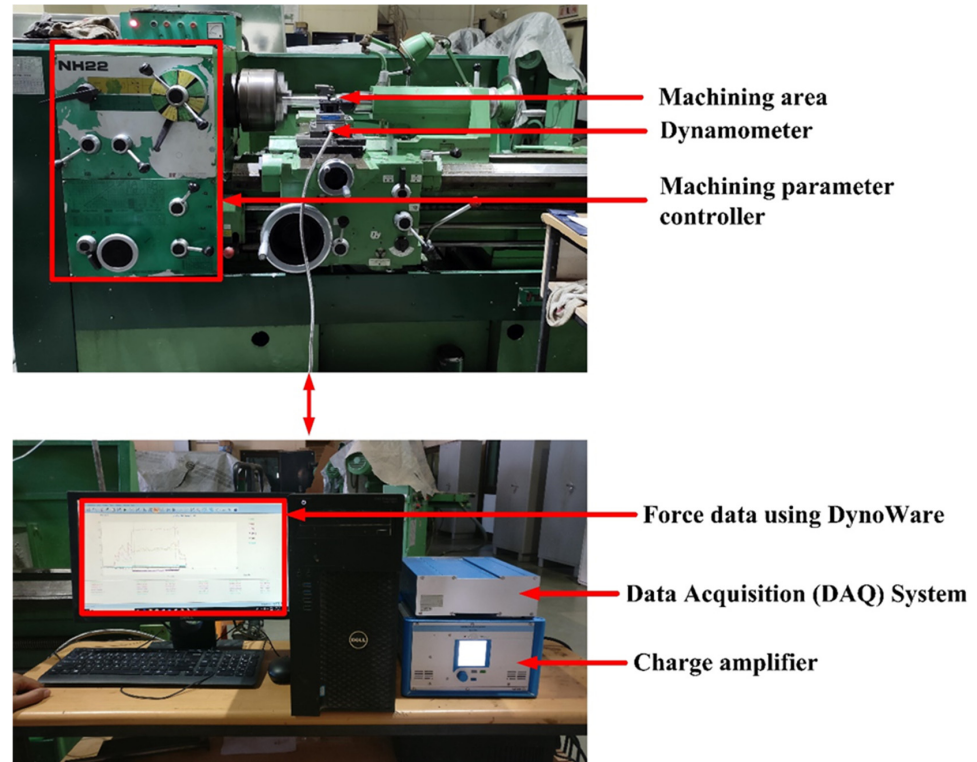
Figure 1. Photographic view of the machining setup with the dynamometer arrangement.

2.3. Design of the Experiment

The machining of the materials was performed using various input parameters. The experimental design helped collect the maximum amount of information for the determination of responses (cutting force and surface roughness) in relation to control factors (cutting speed, feed rate, and depth of cut). The experimental data derived the empirical relations among the control factors and responses. In the present study, the machinability analysis of the RZ5/8 wt.% TiB_2 composite was performed using a standard orthogonal array based on the control factors and levels (low, medium, and high). The detailed machining parameters with the levels considered in the current study are presented in Table 1. For the estimation of machinability, a full factorial experimental design was performed for the number of control factors and levels using the relation P_n. In this case, the number of control factors (n) was 3, and the number of levels (P) was 3. The experiments were performed for all possible combinations of these levels across all factors. Based on these, 27 sets of experimentations were performed, as shown in Table 2.

Table 1. Machining parameters used during machining of the RZ5/8 wt.% TiB_2 composite.

Machining Parameters	Units	Levels		
		Low-1	Medium-2	High-3
Cutting speed	m/min	50	100	150
Feed rate	mm/rev	0.12	0.24	0.36
Depth of cut	mm	0.5	0.75	1.0

**Table 2.** Experimental results for the machinability of the RZ5/8 wt.% TiB$_2$ composite and the S/N ratios.

Run Order	Levels			Average Cutting Force (N)	Average Surface Roughness (μm)	S/N Ratio for Cutting Force	S/N Ratio for Surface Roughness
	Cutting Speed (m/min)	Feed Rate (mm/rev.)	Depth of Cut (mm)				
1	50	0.12	0.5	34.840	0.989	−30.8476	0.0935
2	50	0.12	0.75	55.505	1.105	−34.8916	−0.8714
3	50	0.12	1	67.925	1.411	−36.6407	−2.9894
4	50	0.24	0.5	54.030	2.568	−34.6598	−8.1925
5	50	0.24	0.75	73.805	2.923	−37.3618	−9.3177
6	50	0.24	1	102.600	3.213	−40.2241	−10.1394
7	50	0.36	0.5	74.345	3.726	−37.4296	−11.4240
8	50	0.36	0.75	112.000	4.052	−40.9859	−12.1527
9	50	0.36	1	129.800	4.198	−42.2694	−12.4601
10	100	0.12	0.5	38.905	0.889	−31.8055	1.0140
11	100	0.12	0.75	55.320	1.098	−34.8622	−0.8233
12	100	0.12	1	72.750	1.352	−37.2419	−2.6187
13	100	0.24	0.5	58.125	2.236	−35.2874	−6.9891
14	100	0.24	0.75	84.745	2.732	−38.5765	−8.7297
15	100	0.24	1	105.850	2.869	−40.4963	−9.1557
16	100	0.36	0.5	84.570	3.356	−38.5497	−10.5176
17	100	0.36	0.75	118.975	3.659	−41.5119	−11.2676
18	100	0.36	1	135.450	3.898	−42.6389	−11.8170
19	150	0.12	0.5	42.050	0.898	−32.4884	0.9221
20	150	0.12	0.75	62.370	1.083	−35.9100	−0.6903
21	150	0.12	1	83.110	1.302	−38.3975	−2.2948
22	150	0.24	0.5	62.265	2.299	−35.8924	−7.2335
23	150	0.24	0.75	87.845	2.679	−38.8764	−8.5589
24	150	0.24	1	113.350	2.858	−41.0886	−9.1204
25	150	0.36	0.5	105.415	3.112	−40.4646	−9.8612
26	150	0.36	0.75	138.750	3.467	−42.8447	−10.7985
27	150	0.36	1	149.175	3.995	−43.4750	−12.0300

2.4. Regression Analysis through Taguchi and ANOVA

The machining of the RZ5/8 wt.% TiB$_2$ composite was performed with variations of the control factors, and the machinability was analyzed in terms of cutting force and surface roughness (R$_a$). The typical experimental data generated using a piezoelectric dynamometer are shown in Figure 2 for a specific machining condition. The cutting force shown in the graph in Figure 2 was measured at a cutting speed of 100 m/min, a feed rate of 0.36 m/rev, and a depth of cut of 0.5 mm. Similarly, the cutting force under different machining conditions was measured, and the average cutting force (N) is presented in Table 2 based on the two sets of the experiment. Similarly, average surface roughness (μm) was measured and is presented in Table 2 based on the two sets of the experiment. Control factor effects and quality characteristics in regard to the machinability of the RZ5/8 wt.% TiB$_2$ composite were analyzed using the Taguchi technique. For the statistical analysis, the experimental machinability result was converted into a signal-to-noise ratio (S/N ratio), and the machinability of the materials was investigated in terms of lower-the-better quality characteristics. The S/N ratio for cutting force and surface roughness is presented in Table 2. The lower-the-better quality characteristics help to achieve better machinability properties and ascertain the control factors that significantly affect the material's cutting force and surface roughness.

$$S/N \ ratio = -10 \ Log \frac{1}{n}\left(Y_1^2 + Y_2^2 + Y_3^2 + \ldots + Y_n^2\right) \tag{1}$$

where $Y_1, Y_2, \ldots, Y_n$ = the responses to sliding wear and n = the number of observations.
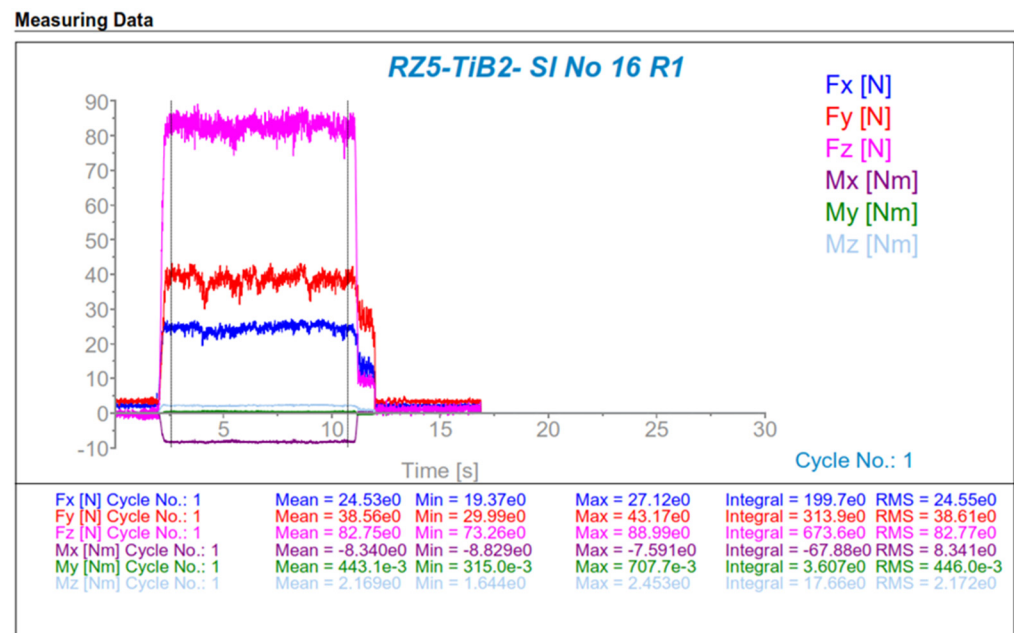
Figure 2. Measurement of cutting force using a Kistler piezoelectric dynamometer at a cutting speed of 100 m/min, a feed rate of 0.36 mm/rev, and a depth of cut of 0.5 mm.

Minitab 17 software was used for the full factorial regression analysis of the experimental cutting force and surface roughness data using the analysis of variance (ANOVA) technique. The regression model estimated the cutting force and surface roughness under different machining conditions. The empirical relations were established for the regression analysis based on the machining control factors and responses. The responses could be estimated according to the experimental data using two control factors, which can be written as Equation (2).

$$Y = \beta_0 + \beta_1 \ X_1 + \beta_2 \ X_2 + \beta_{12} X_1 X_2 + \varepsilon \tag{2}$$

where Y = the response to the control factors; X_1 and X_2 = control factors; and β_0, β_1, β_2, and β_{12} = unknown parameters; and ε = an error term.

The effects of the machining control factors on the responses were determined through main effects plots. These helped to establish the relationships between the single machining control factors and machinability (cutting force and surface roughness). The combined effect of the machining parameters on cutting force and surface roughness was established through the surface response plots by complete quadratic analysis using Minitab 17 software. The statistical regression equation was validated through machining experiments under different operating conditions. A similar approach was used to estimate the tribological behavior of the RZ5/TiB$_2$ magnesium matrix composite under the other operating conditions described in our previous study [30]. The chip morphology and wear of the cutting tool post-machining were analyzed using the ZEISS MERLIN Compact field emission scanning electron microscope (FESEM).

3. Results and Discussions

3.1. Regression Analysis Using the Taguchi Technique

Different machining parameters have different rates of effect on the machinability of materials, such as cutting force and surface roughness. In the present study, a Taguchi analysis was used to ascertain the control factor that had a maximum impact on the machinability of the RZ5/8 wt.% TiB$_2$ composite. The most influential factor on machinability was determined by considering the S/N ratio from the experimental data set. The S/N ratio for the RZ5/8 wt.% TiB$_2$ composite under different machining parameters is presented

in Table 2. The response table for the S/N ratio is given based on the lower-the-better quality characteristics for cutting force and surface roughness. The influences of the input machining parameters are ranked based on the value of the S/N ratio. The response table for the S/N ratio of cutting force shown in Table 3 indicates that the feed rate had the maximum influence in determining the cutting force, followed by the depth of cut and cutting speed during the machining of the RZ5/8 wt.% TiB$_2$ composite. The response for surface roughness shown in Table 4 also indicates that the feed rate had maximum influence and that cutting speed had the minimum impact on the surface roughness of the machined surface.

Table 3. Response table for the S/N ratio of cutting force of the RZ5/8 wt.% TiB$_2$ composite.

Level	Cutting Speed (m/min)	Feed Rate (mm/rev.)	Depth of Cut (mm)
1	−37.2567	−34.7873	−35.2694
2	−37.8856	−38.0515	−38.4246
3	−38.8264	−41.1300	−40.2747
Delta	1.5697	6.3427	5.0053
Rank	3	1	2

Table 4. Response table for the S/N ratio of surface roughness of the RZ5/8 wt.% TiB$_2$ composite.

Level	Cutting Speed (m/min)	Feed Rate (mm/rev.)	Depth of Cut (mm)
1	−7.4948	−0.9176	−5.7987
2	−6.7672	−8.6041	−7.0234
3	−6.6295	−11.3699	−8.0695
Delta	0.8653	10.4523	2.2708
Rank	3	1	2

3.2. Regression Modeling Using the ANOVA Design

3.2.1. ANOVA for Cutting Force

An analysis of variance (ANOVA) was carried out for the cutting force of the RZ5/8 wt.% TiB$_2$ composite and is presented in Table 5. It can be noted that the *p*-value for individual machining parameters (i.e., cutting speed, feed rate, and depth of cut) was 0.000, which indicates a significant influence on cutting force. The *p*-value for the square effect of feed rate and the two-way interactions of Speed × Feed and Feed × DoC was less than 0.05. As the *p*-value was very low, it can be noted that these factors also significantly affected the cutting force of the RZ5/8 wt.% TiB$_2$ composite. Other interactions, such as Speed × Speed, DoC × DoC, and Speed × DoC, had *p*-values greater than 0.05; hence, their influences on the cutting force of the RZ5/8 wt.% TiB$_2$ composite were much lesser.

Table 5. ANOVA for the cutting force of the RZ5/8 wt.% TiB$_2$ composite using adjusted SS for tests.

Source	DF	Adj. SS	Adj. MS	F-Value	*p*-Value
Model	9	26,709.3	2967.7	150.64	0.000
Linear	3	26,157.6	8719.2	442.58	0.000
Speed	1	1080.8	1080.8	54.86	0.000
Feed	1	15,943.3	15,943.3	809.26	0.000
Depth of cut (DoC)	1	9133.4	9133.4	463.60	0.000
Square	3	212.4	70.8	3.59	0.035
Speed × Speed	1	29.3	29.3	1.49	0.239
Feed × Feed	1	107.0	107.0	5.43	0.032
DoC × DoC	1	76.0	76.0	3.86	0.066
Two-way interaction	3	339.3	113.1	5.74	0.007
Speed × Feed	1	191.5	191.5	9.72	0.006
Speed × DoC	1	0.1	0.1	0.01	0.938
Feed × DoC	1	147.7	147.7	7.50	0.014
Error	17	334.9	19.7		
Total	26	27,044.4			

S = 4.43859, R−Sq. = 98.76 %, R−Sq. (adj.) = 98.11 %, R−Sq. (pred.) = 96.71 %.

A regression equation was created to ascertain the cutting force during the machining of the RZ5/8 wt.% TiB$_2$ composite under different machining parameters using Minitab 17 software. As per Table 5, the effects of individual factors and the interactions between other machining parameters were considered to determine the cutting force of the material. Equation (3) gives the regression equation for cutting force estimation.

Regression equation for the cutting force of the RZ5/8 wt.% TiB$_2$ composite in uncoded units:

$$\text{Cutting force} = -29.1 - 0.176\ \text{Speed} - 47.1\ \text{Feed} + 148.3\ \text{DoC} + 0.000884 \\ (\text{Speed} \times \text{Speed}) + 293\ (\text{Feed} \times \text{Feed}) - 57.0\ (\text{DoC} \times \text{DoC}) + 0.666\ (\text{Speed} \times \\ \text{Feed}) - 0.008\ (\text{Speed} \times \text{DoC}) + 117.0\ (\text{Feed} \times \text{DoC}) \tag{3}$$

3.2.2. ANOVA for Surface Roughness

ANOVA was carried out for the surface roughness of the RZ5/8 wt.% TiB$_2$ composite and is presented in Table 6. It can be noted that the *p*-value for all the machining parameters was 0.000, which indicates a significant influence on the surface roughness of the material. The square interaction of DoC × DoC did not have a significant effect, since the *p*-value is more than 0.05. Similarly, the two-way interaction of Speed × DoC, also, did not have a substantial impact, as the *p*-value was 0.289. It is well known that a *p*-value greater than 0.05 has a minimal effect on the prediction of material properties. Other square interactions and two-way interactions with *p*-values less than 0.05 significantly affected the surface roughness of the RZ5/8 wt.% TiB$_2$ composite.

Table 6. ANOVA for surface roughness of the RZ5/8 wt.% TiB$_2$ composite using adjusted SS for tests.

Source	DF	Adj. SS	Adj. MS	F-Value	*p*-Value
Model	9	32.7043	3.6338	553.68	0.000
Linear	3	31.9989	10.6663	1625.21	0.000
Speed	1	0.3453	0.3453	52.61	0.000
Feed	1	30.2525	30.2525	4609.54	0.000
Depth of cut (DoC)	1	1.4011	1.4011	213.49	0.000
Square	3	0.5508	0.1836	27.98	0.000
Speed × Speed	1	0.0533	0.0533	8.13	0.011
Feed × Feed	1	0.4941	0.4941	75.29	0.000
DoC × DoC	1	0.0034	0.0034	0.51	0.483
Two-way interaction	3	0.1545	0.0515	7.85	0.002
Speed × Feed	1	0.1158	0.1158	17.65	0.001
Speed × DoC	1	0.0079	0.0079	1.20	0.289
Feed × DoC	1	0.0308	0.0308	4.69	0.045
Error	17	0.1116	0.0066		
Total	26	32.8158			

S = 0.0810125, R−Sq. = 99.66 %, R−Sq. (adj.) = 99.48 %, R−Sq. (pred.) = 99.06 %.

Equation (4) is the regression equation used to estimate the surface roughness of the RZ5/8 wt.% TiB$_2$ composite, taking the specific and mixed effects of the machining parameters into consideration.

Regression equation for surface roughness of the RZ5/8 wt.% TiB$_2$ composite in uncoded units:

$$\text{Surface roughness} = -1.411 - 0.00792\ \text{Speed} + 20.74\ \text{Feed} + 1.075\ \text{DoC} + \\ 0.000038\ (\text{Speed} \times \text{Speed}) - 19.93\ (\text{Feed} \times \text{Feed}) - 0.380\ (\text{DoC} \times \text{DoC}) - \\ 0.01637\ (\text{Speed} \times \text{Feed}) + 0.00205\ (\text{Speed} \times \text{DoC}) + 1.689\ (\text{Feed} \times \text{DoC}) \tag{4}$$

3.3. Main Effects and Surface Response Plots

3.3.1. Main Effects Plots for Cutting Force and Surface Roughness

Figure 3a depicts the main effects plot for cutting force. It can be observed from the figure that cutting force increased with the increase in machining parameters, such as cutting speed, feed rate, and depth of cut. However, it can be noted that the cutting force was more sensitive to feed rate and depth of cut. At higher feed rates and depths of cut, friction at the tool–workpiece interface and the rate of materials removal were significantly higher, increasing the cutting force of the materials. It can also be seen from the figure that the cutting speed had a lesser influence on the cutting force during the machining of the RZ5/8 wt.% TiB_2 composite.
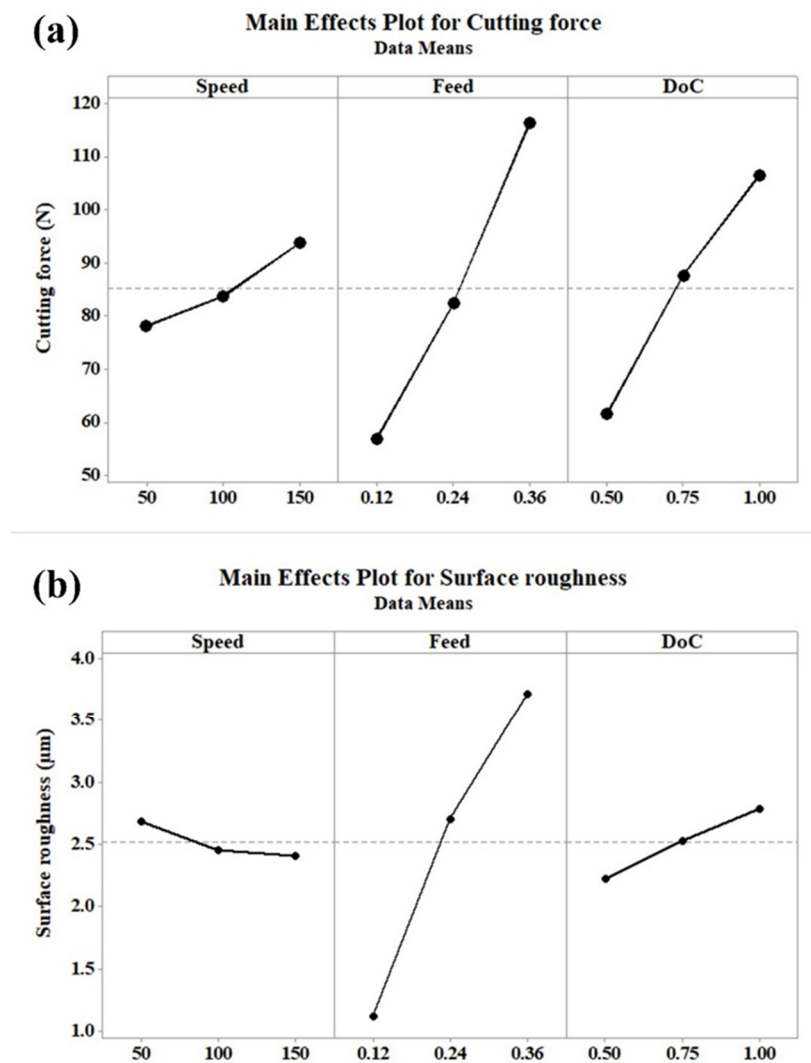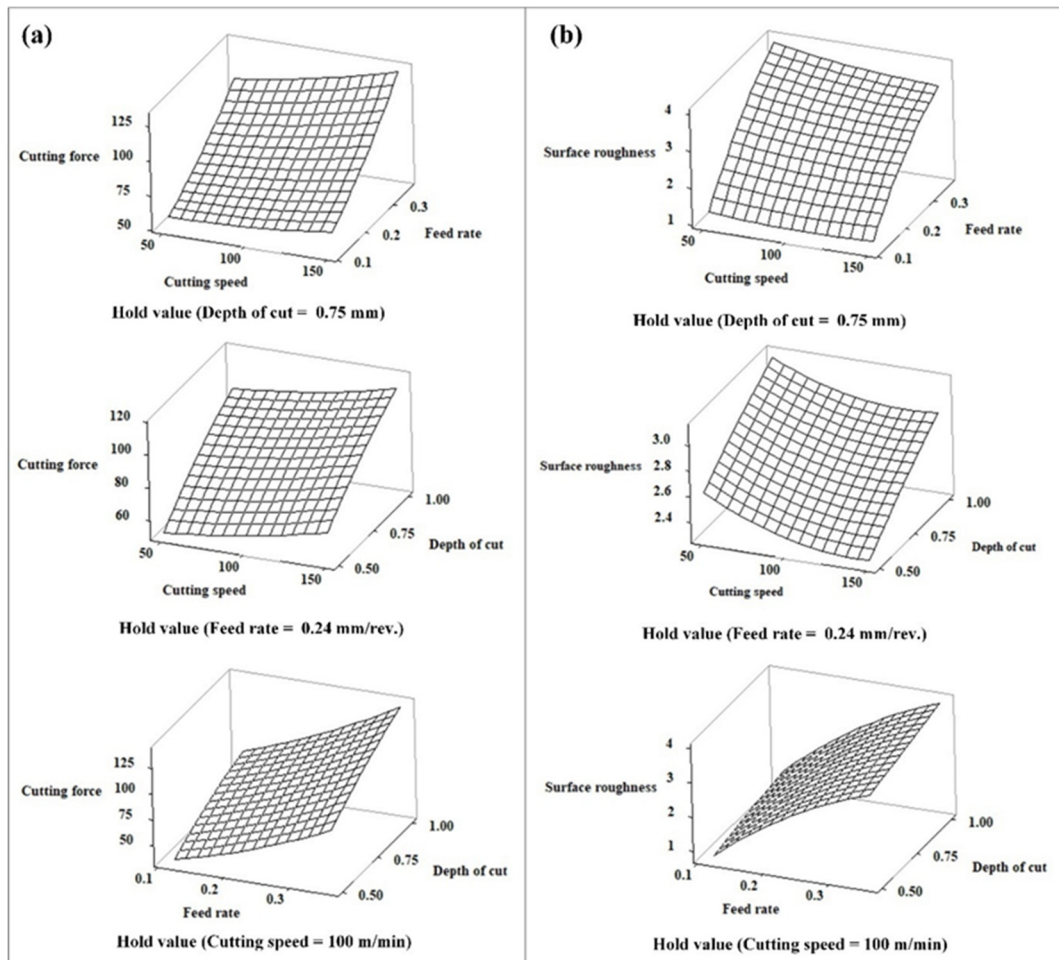

Figure 3. Main effects plots for (**a**) cutting force and (**b**) surface roughness of the RZ5/8 wt.% TiB_2 composite.

Figure 3b depicts the main effects plot for surface roughness. From the figure, it can be seen that the surface roughness of the materials increased significantly with an increase in feed rate. Thrust and the frictional force between the tool and the workpiece were higher at a higher feed rate, resulting in more vibration during machining. Hence, the surface roughness of the materials increased. It was also inferred that cutting speed and depth of cut affected surface roughness marginally. During the machining of the materials, a modest decrease in surface roughness was observed as the cutting speed was increased. However, the surface roughness (R_a) increased as the depth of cut increased.

3.3.2. Response Surface Plots for Cutting Force and Surface Roughness

Figure 4a shows the response surface plot for the cutting force of the RZ5/8 wt.% TiB$_2$ composite. The joint effect of the machining characteristics on the cutting force of the materials can be observed in the figure. The shape of the wireframe of the response surface plot explains the probable location of the individual and combined effects of the input machining parameters on cutting force. It can be observed from the figure that the cutting force of the materials increased for all machining parameters. However, the slope of the plot varies, which indicates that the influences of the machining parameters were not all of the same intensity.
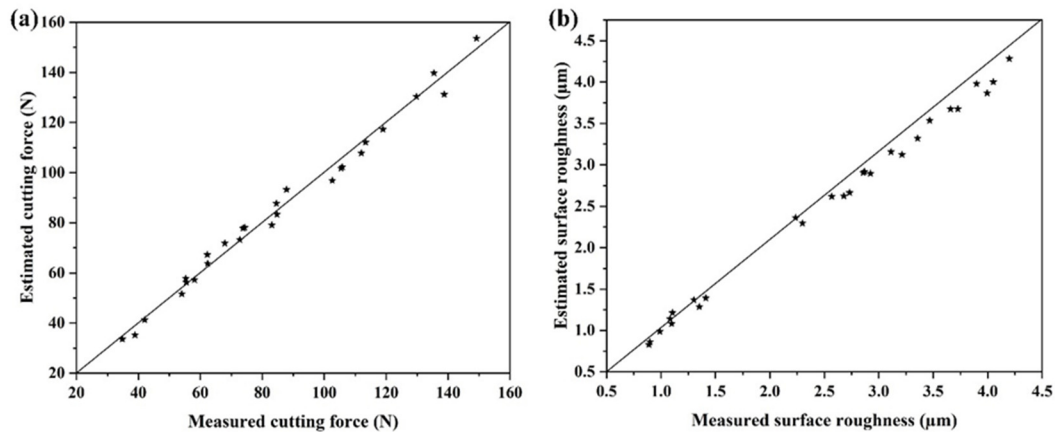

Figure 4. Response surface plots for (**a**) cutting force and (**b**) surface roughness of the RZ5/8 wt.% TiB$_2$ composite.

Similar to the response surface plot for cutting force, the wireframe response surface plots for the surface roughness of the RZ5/8 wt.% TiB$_2$ composite are shown in Figure 4b. The optimal value of the surface roughness of the materials can be determined from the response plots. From the figure, it can be observed that surface roughness has an inverse relationship with cutting speed. However, feed rate and depth of cut directly influence the surface roughness of the materials.

3.4. Validation of the Developed Regression Models

Surface roughness (R$_a$) and cutting force were estimated using the developed regression equations established by the analysis of variance. Figure 5a,b illustrate the variation between estimated and measured values based on various machining parameters. These values were compared with the mean values for cutting force and surface roughness for the

RZ5/8 wt.% TiB$_2$ composite. A linear relationship between the estimated and measured values for cutting force and surface roughness can be observed in the figures. The percentage deviation between the experimentally measured and regression-estimated values was determined for all experimental conditions. Figure 6 indicates the percentage deviation for the cutting force and surface roughness of the RZ5/8 wt.% TiB$_2$ composite. The graph shows the cutting force variation from −8.05 to 9.47%. Considering the surface roughness, the percentage deviation between the experimental and estimated values lay between −9.77 and 6.78%. All the deviation values lay in the range of ±10%, this being considered the acceptable approximation range.

Figure 5. Experimental and regression-estimated response for (**a**) cutting force and (**b**) surface roughness of the RZ5/8 wt.% TiB$_2$ composite.
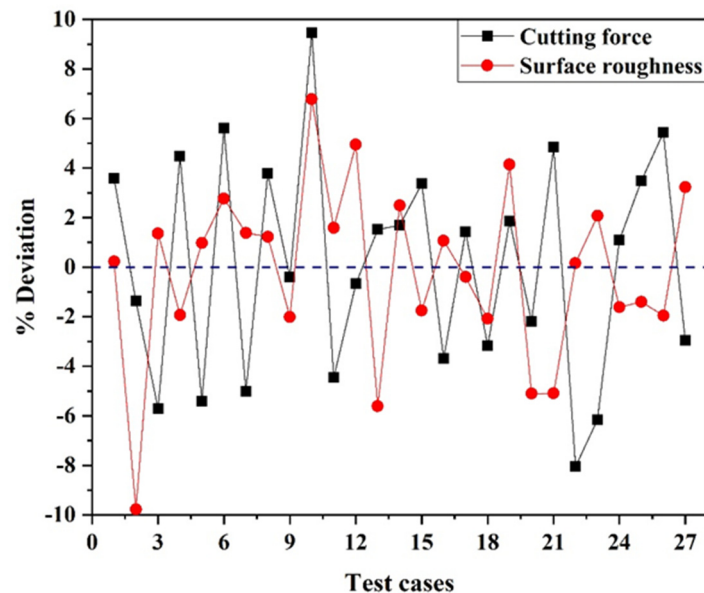
Figure 6. Deviation (%) between experimental and estimated results for cutting force and surface roughness in different test cases.

The confirmation test for the measurement of cutting force and surface roughness was carried out for some sets of machining parameters. Comparison of the experimental and estimated values was based on the mathematical regression model shown in Equations (3) and (4) and presented in Table 7. From the comparative analysis, the error value for cutting force was found to be in the range of −2.33 to 6.88%, and for surface roughness, the error value lay in the range of −4.96 to 3.50%, which was within the acceptable range.

Table 7. Difference between the experimental and estimated values for cutting force and surface roughness, with percentage error calculations.

| Sl. No.	Cutting Speed (m/min)	Feed Rate (mm/rev)	Depth of Cut (mm)	Experimental Cutting Force (N)	Estimated Cutting Force (N)	PERCENTAGE Error of Cutting Force	Experimental Surface Roughness (μm)	Estimated Surface Roughness (μm)	Percentage Error of Surface Roughness
1	75	0.12	0.6	42.76	43.76	−2.33	1.021	0.985	3.50
2	90	0.24	1	98.68	100.84	−2.19	3.009	2.945	2.13
3	136	0.24	0.5	65.86	64.02	2.79	2.351	2.295	2.40
4	110	0.24	0.8	94.32	89.31	5.31	2.592	2.697	−4.03
5	60	0.28	0.7	84.55	82.97	1.87	3.165	3.204	−1.22

3.5. Tool Wear and Chip Morphology

Machining of the RZ5/8 wt.% TiB$_2$ composite indicated abrasive tool wear due to the presence of the TiB$_2$ ceramic particles, and the stress at the tooltip increased due to the discontinuous load of two different phases. Figure 7a,b indicate the wear on both the rake surface and the flank face after the machining of the RZ5/8 wt.% TiB$_2$ composite at a cutting speed of 100 m/min, a feed rate of 0.12 mm/rev, and a depth of cut of 0.5 mm. Abrasive wear is the primary wear mechanism that occurs during the machining of metal matrix composites (MMCs), whereas wear on the flank face is the dominant mode of tool wear. Machining the MMCs at the high cutting speed led to scrap and shock of the cutting tool more effectively due to the ceramic reinforcement, leading to brittle breakage of the tooltip [31]. Narrow grooves were observed at the flank face of the tool, as shown in Figure 7b, due to friction between the flank face and the reinforcement particles. The combined action of cutting force and increased temperature due to friction leads to gradual nose deformation and chipping of the tooltip. Chipping of the cutting tool also sometimes leads to crater formation, either on the rake surface or the flank face of the tool [32].
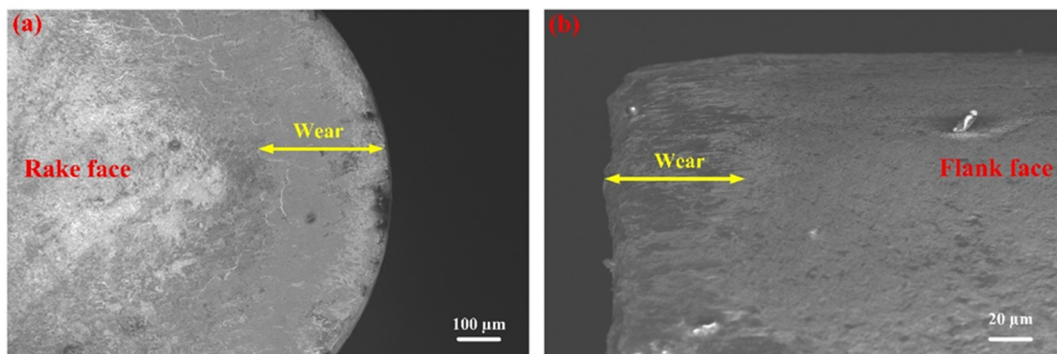
Figure 7. Tool wear after machining of the RZ5/8 wt.% TiB$_2$ composite, with (**a**) the rake face and (**b**) the flank face indicated.

The chip morphologies at different cutting speeds during the machining of the RZ5/8 wt.% TiB$_2$ composite are shown in Figure 8a,b. It can be observed from the FE-SEM micrographs that, for the cutting speed of 50 m/min, the chip morphology exhibited segment formation on both the inner and outer surfaces of the chip. The formation of the segments at the edge of the chip led to the formation of discontinuous chips. Dabade et al. observed materials to behave in a brittle manner, with less influence of either strain rate or temperature at a lower cutting speed. This led to the formation of discontinuous segmented chips during the machining of metal matrix composites [33]. As the cutting speed increased to 100 m/min, the chip morphology evolved to a semi-continuous chip with a helical spring-type structure due to the segmented outer surface and joined inner surface. Helical-structured chips were generated due to the significant change in strain between the outer and inner edges of the chips. Davis et al. observed that, at a lower cutting speed, cracks were initiated at the free surface and propagated toward the tooltip, leading to chip breakage during magnesium matrix composite machining. Semi-continuous chips

were formed at a higher cutting speed due to greater change in strain and as the cracks during machining were initiated at the tooltip and propagated toward the free surface [34].
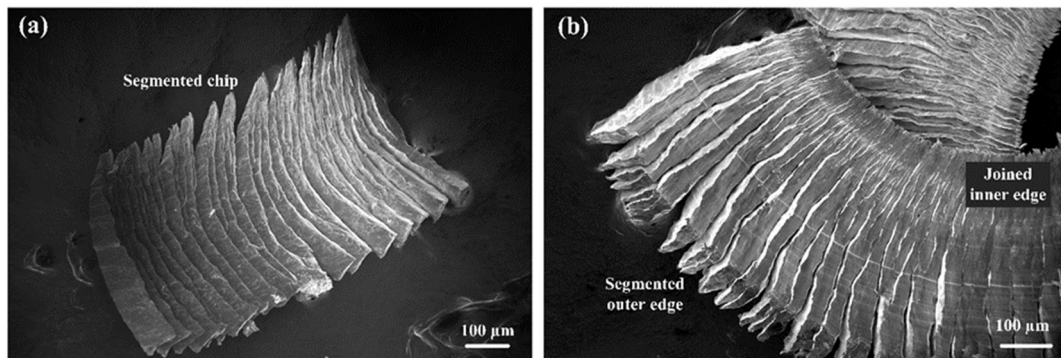
Figure 8. Chip morphologies during machining of the RZ5/8 wt.% TiB$_2$ composite at cutting speeds of (**a**) 50 m/min and (**b**) 100 m/min.

4. Conclusions

The machinability of the RZ5/8 wt.% TiB$_2$ in-situ metal matrix composite was statistically analyzed in the current study with variations in feed rate, cutting speed, and depth of cut. The conclusions drawn are stated below.

1. Taguchi analysis of the machinability of the RZ5/8 wt.% TiB$_2$ composite indicated that feed rate is the most influential factor in determining both the cutting force and surface roughness of the RZ5/8 wt.% TiB$_2$ composite, and cutting speed is the least influential factor.

2. The impacts of machining characteristics on cutting force and surface roughness during machining were analyzed through main effects plots and response surface plots. The cutting force of the RZ5/8 wt.% TiB$_2$ composite increased with feed rate, cutting speed, and depth of cut. The surface roughness also increased with an increase in feed rate and depth of cut, whereas it decreased with an increase in cutting speed.

3. The full factorial design of the experimental data involved the use of the ANOVA technique. A regression model was established to estimate the cutting force and surface roughness of the RZ5/8 wt.% TiB$_2$ composite under different machining conditions. The regression model was validated experimentally with several test cases, and good agreement was observed.

4. The tool wear and chip morphology of the RZ5/8 wt.% TiB$_2$ composite were analyzed under different machining conditions. FESEM micrographs of the cutting tool indicated the abrasive wear on the rake surface and flank face of the cutting tool due to the TiB$_2$ reinforcement.

Author Contributions: Conceptualization, A.M. and M.M.M.; methodology, A.M. and M.M.M.; software, A.M., M.M.M., P.S. and P.R.V.; validation, A.M., M.M.M. and P.S.; formal analysis, A.M., P.S. and K.V.S.; investigation, A.M., M.M.M., P.S. and K.V.S.; resources, M.M.M. and P.R.V.; data curation, A.M.; writing—original draft preparation, A.M.; writing—review and editing, A.M., M.M.M., P.S., P.R.V. and K.V.S.; visualization, A.M. and K.V.S.; supervision, M.M.M. and P.R.V.; project administration, M.M.M.; funding acquisition, K.V.S. All authors have read and agreed to the published version of the manuscript.

Institutional Review Board Statement: Not applicable.

Informed Consent Statement: Not applicable.

Data Availability Statement: The data presented in this study are available upon request from the corresponding author.

Conflicts of Interest: The authors declare no conflict of interest.

References

1. Ceschini, L.; Dahle, A.; Gupta, M.; Jarfors, A.E.W.; Jayalakshmi, S.; Morri, A.; Rotundo, F.; Toschi, S.; Singh, R.A. *Aluminum and Magnesium Metal Matrix Nanocomposites*; Springer: Berlin/Heidelberg, Germany, 2017. [CrossRef]
2. Liu, J.; Suryanarayana, C.; Ghosh, D.; Subhash, G.; An, L. Synthesis of Mg-Al_2O_3 nanocomposites by mechanical alloying. *J. Alloys Compd.* **2013**, *563*, 165–170. [CrossRef]
3. Meher, A.; Mahapatra, M.M.; Samal, P.; Vundavilli, P.R.; Madavan, S. Synthesis, microstructure and mechanical properties of magnesium matrix composites fabricated by stir casting. *Mater. Today Proc.* **2019**, *18*, 4034–4041. [CrossRef]
4. Yao, Y.; Chen, L. Processing of B4C particulate-reinforced magnesium-matrix composites by metal-assisted melt infiltration technique. *J. Mater. Sci. Technol.* **2014**, *30*, 661–665. [CrossRef]
5. Wang, H.Y.; Jiang, Q.C.; Wang, Y.; Ma, B.X.; Zhao, F. Fabrication of TiB_2 particulate reinforced magnesium matrix composites by powder metallurgy. *Mater. Lett.* **2004**, *58*, 3509–3513. [CrossRef]
6. Meher, A.; Chaira, D. Effect of graphite and SiC addition into Cu and SiC particle size effect on fabrication of Cu-Graphite-SiC MMC by powder metallurgy. *Trans. Indian Inst. Met.* **2017**, *70*, 2047–2057. [CrossRef]
7. Wang, H.Y.; Jiang, Q.C.; Zhao, Y.G.; Zhao, F. In-situ synthesis of TiB_2/Mg composite by self-propagating high-temperature synthesis reaction of the Al-Ti-B system in molten magnesium. *J. Alloys Compd.* **2004**, *379*, L4–L7. [CrossRef]
8. Chawla, K.K. *Composite Materials Science and Engineering*; Springer: Berlin/Heidelberg, Germany, 2012. [CrossRef]
9. Tjong, S.C. Microstructural and mechanical characteristics of in-situ metal matrix composites. *Mater. Sci. Eng. R Rep.* **2000**, *29*, 49–113. [CrossRef]
10. Sahoo, B.N.; Panigrahi, S.K. Synthesis, characterization and mechanical properties of in-situ (TiC-TiB_2) reinforced magnesium matrix composite. *Mater. Des.* **2016**, *109*, 300–313. [CrossRef]
11. Meher, A.; Mahapatra, M.M. *The Tribological Behavior of an In-Situ Processed Magnesium Alloy-Based Metal Matrix Composite*; Springer International Publishing: Berlin/Heidelberg, Germany, 2021; pp. 75–89. [CrossRef]
12. Samal, P.; Vundavilli, P.R.; Meher, A.; Mahapatra, M.M. Recent progress in aluminum metal matrix composites: A review on processing, mechanical and wear properties. *J. Manuf. Process.* **2020**, *59*, 131–152. [CrossRef]
13. Meher, A.; Mahapatra, M.M.; Samal, P.; Vundavilli, P.R. Abrasive wear behaviour of TiB_2 reinforced in-situ synthesized magnesium RZ5 alloy based metal matrix composites. *Met. Mater. Int.* **2020**, *27*, 3652–3665. [CrossRef]
14. Kumar, A.; Mahapatra, M.; Jha, P. Effect of machining parameters on cutting force and surface roughness of in-situ Al-4.5%Cu/TiC metal matrix composites. *Measurement* **2014**, *48*, 325–332. [CrossRef]
15. Manna, A.; Bhattacharayya, B. Influence of machining parameters on the machinability of particulate reinforced Al/SiC-MMC. *Int. J. Adv. Manuf. Technol.* **2005**, *25*, 850–856. [CrossRef]
16. Ozben, T.; Kilickap, E.; Çakır, O. Investigation of mechanical and machinability properties of SiC particle reinforced Al-MMC. *J. Mater. Process. Technol.* **2008**, *198*, 220–225. [CrossRef]
17. Hung, N.; Yeo, S.; Oon, B. Effect of cutting fluid on the machinability of metal matrix composites. *J. Mater. Process. Technol.* **1997**, *67*, 157–161. [CrossRef]
18. Pramanik, A.; Zhang, L.; Arsecularatne, J. Machining of metal matrix composites: Effect of ceramic particles on residual stress, surface roughness and chip formation. *Int. J. Mach. Tools Manuf.* **2008**, *48*, 1613–1625. [CrossRef]
19. Anandakrishnan, V.; Mahamani, A. Investigations of flank wear, cutting force, and surface roughness in the machining of Al-6061-TiB_2 in-situ metal matrix composites produced by flux-assisted synthesis. *Int. J. Adv. Manuf. Technol.* **2011**, *55*, 65–73. [CrossRef]
20. Mukherjee, I.; Ray, P.K. A review of optimization techniques in metal cutting processes. *Comput. Ind. Eng.* **2006**, *50*, 15–34. [CrossRef]
21. Kumar, K.V.; Sait, A.N. Modelling and optimisation of machining parameters for composite pipes using artificial neural network and genetic algorithm. *Int. J. Interact. Des. Manuf. (IJIDeM)* **2017**, *11*, 435–443. [CrossRef]
22. Kumar, P.; Karsh, P.K.; Misra, J.P.; Kumar, J. Multi-objective optimization of machining parameters during green machining of aerospace grade titanium alloy using Grey-Taguchi approach. *Proc. Inst. Mech. Eng. Part E J. Process. Mech. Eng.* **2021**, 09544089211043610. [CrossRef]
23. Karloopia, J.; Mozammil, S.; Jha, P.K. Machinability, modelling and statistical analysis of in-situ Al-Si-TiB_2 composites. *J. Compos. Sci.* **2019**, *3*, 28. [CrossRef]
24. Khanna, N.; Suri, N.M.; Agrawal, C.; Shah, P.; Krolczyk, G.M. Effect of hybrid machining techniques on machining performance of in-house developed Mg-PMMC. *Trans. Indian Inst. Met.* **2019**, *72*, 1799–1807. [CrossRef]
25. Kök, M. Modelling the effect of surface roughness factors in the machining of 2024Al/Al_2O_3 particle composites based on orthogonal arrays. *Int. J. Adv. Manuf. Technol.* **2011**, *55*, 911–920. [CrossRef]
26. Ghandehariun, A.; Kishawy, H.; Balazinski, M. On machining modeling of metal matrix composites: A novel comprehensive constitutive equation. *Int. J. Mech. Sci.* **2016**, *107*, 235–241. [CrossRef]
27. Wang, J.; Zuo, J.; Shang, Z.; Fan, X. Modeling of cutting force prediction in machining high-volume SiCp/Al composites. *Appl. Math. Model* **2019**, *70*, 1–17. [CrossRef]

28. Gürbüz, H.; Gönülaçar, Y.E. Experimental and statistical investigation of the effects of MQL, dry and wet machining on machinability and sustainability in turning of AISI 4140 steel. *Proc. Inst. Mech. Eng. Part E J. Process. Mech. Eng.* **2022**, *236*, 808–1823. [CrossRef]

29. Meher, A.; Mahapatra, M.M.; Samal, P.; Vundavilli, P.R. Study on effect of TiB_2 reinforcement on the microstructural and mechanical properties of magnesium RZ5 alloy based metal matrix composites. *J. Magnes. Alloy* **2020**, *8*, 780–792. [CrossRef]

30. Meher, A.; Mahapatra, M.M. Modeling the abrasive wear behavior of in-situ synthesized magnesium RZ5/TiB2 metal matrix composites. *Proc. Inst. Mech. Eng. Part E J. Process Mech. Eng.* **2022**, *236*, 1500–1510. [CrossRef]

31. Ciftci, I.; Turker, M.; Seker, U. Evaluation of tool wear when machining SiC_p-reinforced Al-2014 alloy matrix composites. *Mater. Des.* **2004**, *25*, 251–255. [CrossRef]

32. Bhushan, R.K.; Kumar, S.; Das, S. Effect of machining parameters on surface roughness and tool wear for 7075 Al alloy SiC composite. *Int. J. Adv. Manuf. Technol.* **2010**, *50*, 459–469. [CrossRef]

33. Dabade, U.A.; Joshi, S.S. Analysis of chip formation mechanism in machining of Al/SiC_p metal matrix composites. *J. Mater. Process. Technol.* **2009**, *209*, 4704–4710. [CrossRef]

34. Davis, B.; Dabrow, D.; Ju, L.; Li, A.; Xu, C.; Huang, Y. Study of Chip Morphology and Chip Formation Mechanism during Machining of Magnesium-Based Metal Matrix Composites. *J. Manuf. Sci. Eng. Trans. ASME* **2017**, *139*, 1–10. [CrossRef]